Research Square

Preprints are preliminary reports that have not undergone peer review.
They should not be considered conclusive, used to inform clinical practice,
or referenced by the media as validated information.

A Pre-Enrichment-Free Colorimetric Biosensor Based on Immunomagnetic Separation and G-Quadruplex DNAzyme Signal Amplification for Ultrasensitive Detection of Vibrio parahaemolyticus in Seafood

Xiaomu Wang
Jilin University
Wenteng Qiao
Jilin University
Boyuan Chen
Jilin University
Pengyue Quan
Jilin University
Yiwa Liu
Guangdong Medical College
Xiuling Song
songxiuling@jlu.edu.cn
Jilin University
Yanli Gao
Jilin University
Li Li
Guangdong Medical College

Research Article

Keywords: Vibrio parahaemolyticus, Chicken yolk antibody, Immunomagnetic separation, G- quadruplex, Colorimetric method

Posted Date: June 19th, 2026

DOI: https://doi.org/10.21203/rs.3.rs-9974970/v1

License: This work is licensed under a Creative Commons Attribution 4.0 International License.
Read Full License

Additional Declarations: No competing interests reported.

Abstract

Vibrio parahaemolyticus a halophilic foodborne pathogen in seafood, threatens food safety and public health, requiring rapid and sensitive detection. Here, a pre-enrichment-free colorimetric sensor was developed for its quantitative detection by integrating immunomagnetic separation, freeze-driven ssDNA modification and G-quadruplex DNAzyme-mediated signal amplification. Fe_3O_4@Ag NPs-apt and AuNPs-IgY specifically captured target bacteria to form a magnet-separable sandwich structure; excess AuNPs-IgY in the supernatant bound to poly-A(15)-labeled ssDNA via freeze-thaw, and free ssDNA hybridized with a hairpin probe to release G-quadruplex sequences. The latter self-assembled with hemin to form peroxidase-mimicking DNAzyme, which catalyzed ABTS-H_2O_2 color reaction for absorbance measurement at 418 nm. Under optimized conditions, the sensor exhibited two linear ranges for *V. parahaemolyticus* in PBS (10~10^5 and 10^5~10^7 CFU/mL, R^2>0.99) with a LOD of 3.02 CFU/mL, and excellent specificity against common foodborne pathogens. For oyster samples, it achieved linear detection (10~10^5 and 10^5~10^7 CFU/mL, R^2>0.99) with a LOD of 54.95 CFU/mL. This method is simple, sensitive, specific and applicable to complex seafood matrices, providing a promising on-site tool for *V. parahaemolyticus* detection and seafood safety assurance.

1. Introduction

Vibrio parahaemolyticus (V. parahaemolyticus) is a non-sporulated, facultative anaerobic, halophilic arc-shaped, rod-shaped or filamentous gram-negative bacterium, which is an opportunistic foodborne pathogen commonly found in freshwater, marine and estuarine aquatic systems worldwide(Ma et al., 2023). It has rapid growth and strong adaptability, and usually attaches to particles or zooplankton(Lovell, 2017). When filter-feeding mollusks such as shellfish filter surrounding water through gills to obtain oxygen and food, *V. parahaemolyticus* is filtered, retained and concentrated together with particulate matter or small plankton, making the consumption of raw or undercooked seafood an infection route for pathogenic *V. parahaemolyticus* (Froelich et al., 2013, Hash et al., 2019). Gastroenteritis is the most common syndrome caused by *V. parahaemolyticus*, with symptoms including diarrhea accompanied by abdominal cramps, nausea, vomiting, headache, chills and low-grade fever; it can also cause sepsis and death in immunocompromised patients (Su and Liu, 2007, Velazquez-Roman et al., 2014). Its pathogenicity mainly stems from two major virulence factors: thermostable direct hemolysin (TDH) and TDH-related hemolysin (TRH), which act on the host cell surface and destroy cell integrity (Zhao et al., 2020). Some pathogenic strains do not produce TRH and TDH but secrete other virulence factors such as protease, siderophore and biofilm (Anupama et al., 2019), while secretion systems T3SS2, T3SS6 and adhesion factors like VpadF also play important roles in pathogenicity(Letchumanan et al., 2014, Liu and Chen, 2015, Liu et al., 2018a).

With the rapid development of logistics and the increasing circulation of seafood, the incidence of *V. parahaemolyticus*-induced diseases has been on the rise in recent years, posing severe global challenges(Li et al., 2019a). Thus, it is urgent to develop a simple, rapid, highly sensitive and specific detection method for *V. parahaemolyticus* to reduce transmission risks. Common detection methods

include traditional isolation, culture and identification, immunological methods based on antigen-antibody binding, and molecular biological methods based on nucleic acid amplification (Duan et al., 2014). However, these existing methods have inherent shortcomings, such as complex sample pretreatment, poor sensitivity, long analysis time, high cost and reliance on expensive instruments (Chen et al., 2021). Two key issues need to be addressed in developing new detection methods: the complexity and time-consuming nature of sample pretreatment and pre-enrichment, and the effective conversion and amplification of detection signals.

In this study, we adopted immunomagnetic separation technology, using magnetic nanoprobes formed by coupling magnetic beads with aptamers to achieve specific enrichment and separation of *V. parahaemolyticus* in a short time. Meanwhile, we integrated G-quadruplex visualization technology by designing a hairpin-structured nucleic acid reporter probe (Hairpin), which encloses the G-quadruplex backbone sequence and single-stranded DNA (ssDNA) complementary sequence in its stem-loop structure. When ssDNA hybridizes with Hairpin to form a double strand, the hairpin opens to release the G-quadruplex sequence, which then self-assembles with hemin in the reaction system to form a G-quadruplex DNAzyme with peroxidase activity. Finally, ABTS solution is added for enzymatic color development, and rapid detection and quantification of *V. parahaemolyticus* are realized by measuring the absorbance with a microplate reader. This study presents a pre-enrichment-free detection method for *V. parahaemolyticus* that significantly improves detection efficiency while realizing signal conversion and amplification, aiming to better meet the demands of rapid detection, food safety and public health.

Scheme1. Schematic diagram of *V. parahaemolyticus* detection method in this study.

2. Materials and Methods

2.1. Determination of IgY Purity by SDS-PAGE

Glass plates were assembled, a comb was inserted, and a mark was drawn 1 cm below the lower edge of the comb. A 5 mL 10% separating gel was prepared according to the instructions, mixed thoroughly, and poured into the gap between the glass plates up to the mark, followed by overlaying with water to keep the gel surface flat. The separating gel was considered polymerized when a clear interface appeared between the gel and the water layer. A 3 mL 5% stacking gel was prepared as per the instructions; after removing the water layer, the stacking gel was injected and the comb was reinserted without generating air bubbles. Once the stacking gel was fully polymerized, the glass plate assembly was mounted into the electrophoresis tank, sufficient running buffer was added, and the comb was gently pulled out. The IgY sample was appropriately diluted, mixed with 2×SDS loading buffer at an equal volume, and boiled for 3–5 min to denature proteins. After cooling to room temperature, 10 μL of the sample was loaded into each well, with 10 μL of protein molecular weight marker loaded as a control. Electrophoresis was performed at 70 V through the stacking gel, then switched to 100 V until the bromophenol blue dye front reached the bottom of the gel, and the power supply was turned off. The gel was separated from the glass plates, placed in a petri dish, stained with Coomassie brilliant blue for 15

min on a shaker, and the staining solution was discarded. Destaining solution was added, and the gel was destained overnight on a shaker until clear protein bands appeared, which were then analyzed, photographed, and stored using a gel imaging system. The grayscale values of the bands were analyzed with ImageJ software, and the protein purity was calculated using the following formula:

$$Proteinpurity\ (\%) = \frac{Heavy\ gray + Light\ gray}{Heavy\ gray + Light\ gray + Impurity\ gray}$$

where Heavy gray refers to the grayscale value of the heavy chain band, Light gray denotes the grayscale value of the light chain band, and Impurity gray represents the grayscale value of impurity protein bands in SDS-PAGE.

2.2. Preparation of used DNA sequences

The thiol-modified aptamer of *V. parahemolyticus* (Apt) was previously reported (Wu et al., 2015). The single strand DNA (ssDNA) and hairpin structure probe (Hairpin) were designed and analysed with the online website NUPACK (https://nupack.org/) and the results are shown in **Fig S1**. When the ssDNA and Hairpin were mixed in equal concentrations under the experimental condition of 37℃, the complementary moiety is able to stably hybridize to form a duplex, leaving the G4 sequence in a free and foldable state. In order to realize the freeze-driven absorption on AuNPs, 15 A bases were labled at the 5' end of the ssDNA (Hu et al., 2020, Ye et al., 2022). The Hairpin contained a reverse complementary sequence of part of ssDNA and the $CatG_4$ sequence. $CatG_4$ could be blocked without the ssDNA due to the formation of the hairpin structure, and instead would dissociated in the presence of the ssDNA. The Apt, ssDNA and Hairpin were synthesized and purified by high performance liquid chromatography at Sangon Biotech (Shanghai, China). **Table S1** shows all the sequences used in this work as well as the product size.

2.3. Synthesis of Fe_3O_4@Ag NPs-apt

The synthesis of Fe_3O_4 NPs were performed according to the previously reported procedure with slight modifications (Zhu et al., 2011), and detailed steps could be found in the published article of our research group(Su et al., 2023). Briefly, 2.16 g $FeCl_3 \cdot 6H_2O$, 0.5 g trisodium citrate and 3.34 g sodium acetate were dissolved in 40 mL ethylene glycol, and accelerated by ultrasonic dissolution for 30 ~ 60 min until completely dissolved. Then, the solution was transferred to a Teflon-lined stainless-steel autoclave, and put in an electric oven at 200℃ for 12 h. After being cooled, the product in autoclave was poured into a beaker, and the black solid particles in it were separated from liquid by magnet, washed with distilled water and anhydrous ethanol alternately. Finally, the Fe_3O_4 NPs was dried in vacuum oven at 60℃ overnight, and stored at 4℃ for later use after grinding.

The Fe_3O_4@Ag NPs were synthesized according to the previous work(Jun et al., 2009). First, 0.2 g Fe_3O_4 NPs, 0.1 g $AgNO_3$ and 2.5 g PVP were dissolved in 24 mL glycol, magnetically stirred at 100℃ for 12 h.

Synthetic brown solid particles were magnetically separated from solution, washed with distilled water and acetone alternatively. Fe_3O_4 @ Ag NPs were finally resuspended in 10 mL distilled water to prepare a stock solution with a concentration of 20 mg/ml, and 10-fold diluted before use.

Finally, Fe_3O_4@Ag NPs-apt were prepared based on the method reported in literature (Abbaspour et al., 2015). First, 4 μL TCEP (10 mM) and 40 μL Apt (10 μM) were mixed in the dark at room temperature for 1 h. Then, the mixture was added into 1 mL Fe_3O_4 @Ag NPs (2 mg/mL) and incubated at room temperature for 20 h avoid light. Finally, Fe_3O_4@Ag NPs-apt were magnetically separated and resuspended in 1 mL 1% BSA for blocking.

2.4. Synthesis of AuNPs-IgY

The preparation of AuNPs was modified according to the citrate reduction method (Liu and Lu, 2006, Li et al., 2019b). First, a mixture of 1 mL 1% $HAuCl_4 \cdot 3\ H_2O$ and 99 mL distilled water was heated and stirred at 200℃. Then, 4 mL 1% trisodium citrate was added into the mixture quickly as soon as it comes to a boil. During 5 min of reaction, the color shifted from pale yellow to colorless to purple to wine-red. Finally, the AuNPs solution was cooled to room temperature and stored at 4℃ avoid light.

The AuNPs-IgY were prepared according to a previous paper(Zhou et al., 2009). IgY against *V. parahaemolyticus* at a titer of 1:128000 was prepared in our own laboratory. First, 1 mL AuNPs solution was centrifuged (12000 r/min, 4℃) for 30 min. Precipitated AuNPs were resuspended in 1 mL distilled water. After adjusting the pH of AuNPs solution with 7 μL K_2CO_3 (0.1 mol/L), 15 μg IgY was added into the solution, and the conjugation was carried out at room temperature for 1 h. Then, the solution was centrifuged (12000 r/min, 4℃) for 30 min. Subsequently, the supernatant of the solution was removed. Finally, AuNPs-IgY were resuspended in 100 mL distilled water.

2.5. Procedure for colorimetric detection of *V. parahemolyticus*

Vibrio parahemolyticus solutions of various concentrations (10^7, 10^6, 10^5, 10^4, 10^3, 10^2, and 10 CFU/mL) were prepared by diluting freshly cultured bacteria solution with sterile PBS. Then, 100 μL *Vibrio parahemolyticus* solution, 40 μL Fe_3O_4@Ag NPs-apt, 40 μL AuNPs-IgY were added into 1.5 mL centrifuge tube, and supplemented with distilled water to a total volume of 200 μL. At the same time, equal volume of distilled water was used to replace *Vibrio parahemolyticus* to set up blank control group. After being gently vortexed at 37℃ for 1 h, the mixture was magnetically separated for 10 min, and the supernatant was transferred and mixed with 10 μL ssDNA (10 μmol/L), frozen at -20℃ for 1 h, followed by thawing at room temperature. Next, the solution was centrifuged (12000 r/min, 4℃) for 30 min, and the supernatant was transferred in to 96-well plate. Subsequently, 10 μL Hairpin (10 μmol/L) was added to hybrid with ssDNA at 37 ℃ for 1 h. Next, 5 μL Hemin (10 μmol/L) and 45 μL buffer solution (150 mM NH_4Cl, 20 mM KCl, 50 mM Tris-HCl, pH = 7) were added and incubated at room temperature for 1 h to

fold CatG4. Finally, 50 μL ABTS solution (12 mM) including 10 mM H_2O_2 was added to be catalyzed at room temperature for 7 min. The absorbance was measured by enzyme-labled instrument.

3. Results and Discussion

3.1. Assay principle

The schematic for the *V. parahaemolyticus* detection method is shown in **Scheme. 1**. The detection principle was mainly based on the peroxidase activity of G4, combining with the technology of magnetic separation and specific recognition ability of aptamer and antibody. In addition, the freezing method was applied to modify poly-A(15) onto the surface of AuNPs. First, Fe_3O_4@Ag NPs-apt and AuNPs-IgY were synthesized and used to catch *V. parahaemolyticus* to form three sandwich structure. Then, excess AuNPs-IgY in the supernatant was separated by magnet and conjuncted with excessive ssDNA which has been labeled fifteen A bases at the 5' end with freezing method. Next, the remaining ssDNA in the supernatant after centrifugation were hybridized with Hairpin to release G4. Finally, Hemin, folding buffer solution with K^+ and NH_4^+, ABTS and H_2O_2 were added successively. The absorbance was measured by enzyme-labeled instrument.

3.2. Antibody Titer, Protein Concentration and Purity Determination

Indirect ELISA was employed to determine the titer of IgY antibodies, which was defined as the maximum dilution factor showing positive results after immobilizing Vibrio parahaemolyticus on 96-well microplates, incubating with serially diluted IgY and enzyme-labeled secondary antibody, and developing color. IgY was extracted from eggs collected weekly starting from the third immunization to plot the titer monitoring curve (Fig. 1a), revealing a titer of 1:128,000 one week after the third immunization, a significant increase to a maximum of 1:256,000 after the fourth immunization, followed by a rapid decline to 1:8,000 possibly due to rapid antigen-induced antibody consumption; the titer rose to 1:128,000 after the fifth immunization, maintained at 1:64,000 after the sixth, and decreased subsequently upon immunization cessation. The BCA protein assay kit was used to quantify IgY concentration, with a standard curve plotted using protein standard concentration as the abscissa and OD_{562} value as the ordinate (Fig. 1c), yielding a linear fitting equation of $y = 0.414x + 0.1227$ ($R^2=0.9974$); the IgY concentration was calculated as 38.09 mg/mL by substituting sample absorbance into the curve and correcting for dilution factor (Fig. 1d). SDS-PAGE analysis confirmed the purity of extracted IgY, whose molecular weight is approximately 180 kDa (heavy chain: 60 ~ 70 kDa; light chain: 22 ~ 30 kDa); as shown in Fig. 1b, the heavy and light chains exhibited expected molecular weights with clear bands and minimal impurities, resulting in a calculated protein purity of 88.63%. These results demonstrate that the prepared IgY antibodies possess satisfactory titer, appropriate concentration and high purity, meeting the requirements for subsequent experimental applications.

3.2. Characterization

To verify the structural integrity and functional modification efficiency of the prepared nanomaterials, multiple characterization methods were utilized to investigate. The surface morphology and particle size of Fe_3O_4@Ag NPs and Fe_3O_4@Ag NPs-apt were characterized by transmission electron microscopy. Figure 2a and Fig. 2b shows the transmission electron microscopy images of Fe_3O_4@Ag NPs and Fe_3O_4@Ag NPs-apt, respectively. Fe_3O_4@Ag NPs was roughly spherical and covered with a thin transparent layer after its surface was modified with aptamer. Radius software was used to measure particle sizes. **Fig S2a** and **Fig S2b** shows the particle size distributions of Fe_3O_4@Ag NPs and Fe_3O_4@Ag NPs-apt, respectively. After linear fitting of the bar graph, mean particle sizes of Fe_3O_4@Ag NPs and Fe_3O_4@Ag NPs-apt were (99.34 ± 20.55) nm and (107.83 ± 25.43) nm. **Fig S3** shows the EDS element distribution map of Fe_3O_4@Ag NPs, and three elements Fe, O and Ag were simultaneously present in the scanning area. The crystal composition of Fe_3O_4@Ag NPs was characterized by X-ray diffraction. The results are shown in Fig. 2j from 2θ = 20° to 80°. The position and relative intensity of the peaks observed at 2θ of 30.3°, 35.6°, 43.2°, 57.2° and 62.9° matched exactly with Fe_3O_4 (JCPDS card: 75 – 1609). The diffraction peaks at 2θ of 38.2°, 44.3°, 64.5° and 77.4° corresponded to the face-centered cube of Ag (JCPDS card: 04-0783). The magnetic properties of the fabricated magnetic nanoparticles were characterized using a vibrating sample magnetometer. The results are shown in Fig. 2i The magnetic saturation (MS) values of Fe_3O_4 NPs, Fe_3O_4@Ag NPs, and Fe_3O_4@Ag NPs-apt were 57.6 emu/g, 49.3 emu/g, and 43.6 emu/g, respectively. The reduction of MS indicates that AgNPs and aptamers are deposited sequentially on the surface of Fe_3O_4 NPs. The potentials of Fe_3O_4@Ag NPs and Fe_3O_4@Ag NPs-apt were characterized by potential analyzer. As shown in **Fig S4**, surface potential of Fe_3O_4@Ag NPs is -5.60 ± 0.05, which decreases to -14.73 ± 0.15 after modification of electronegative aptamer.

The surface morphology and particle size of AuNPs and AuNPs-IgY were characterized by transmission electron microscopy. As shown in Fig. 2c, the spherical AuNPs were uniformly distributed. After the modification of the antibody against *V. parahaemolyticus (*Fig. 2d**)**, a thin transparent layer could be seen on its surface. The particle sizes of AuNPs and AuNPs - IgY are (15.55 ± 1.48) nm and (19.70 ± 1.88) nm, respectively (**Fig S2c and S2d**). **Fig S5** shows that the maximum absorption peak of AuNPs in the UV-Vis region is 520 nm, and the red solution is uniformly transparent without impurities. After modifying antibody against *V. parahaemolyticus*, the absorption peak shifts to 522 nm. The co-incubation mixtures of Fe_3O_4@Ag NPs-apt, AuNPs-IgY and *V. parahaemolyticus* were characterized by transmission electron microscopy, and the results are shown in **Fig S6**. Fe_3O_4@Ag NPs-apt and AuNPs-IgY were bound to the bacterial surface. These results indicate that Fe_3O_4@Ag NPs-apt and AuNPs-IgY can simultaneously capture *V. parahaemolyticus* to form a sandwich structure. Figure 2e - h shows the EDS map of element distribution of the three - sandwich structure. The results indicate the presence of three elements, Fe, Ag, and Au. Collectively, these characterization results validate the successful construction of the Fe_3O_4@Ag NPs-apt/*V. parahaemolyticus*/Au NPs-IgY sandwich structure, laying a solid foundation for the subsequent development of the colorimetric sensing platform.

3.3. Condition optimization

To optimize the colorimetric detection performance of the developed sensing platform, systematic investigations of key reaction conditions were subsequently conducted. Different dosages of Fe_3O_4@Ag NPs-apt ranging from 10 to 50 μL were set to enrich *V. parahaemolyticus* with a concentration of 1×10^7 CFU/mL. The supernatant liquid was gradient diluted and coated on a plate after magnetic separation. The results are shown in Fig. 3a and **Fig S7**. The enrichment efficiency increased gradually with the increase of the dosage of Fe_3O_4@Ag NPs-apt. When the dosage was 40 μL, the enrichment efficiency reached 99.26% and did not further improve significantly. This indicates that most of the bacteria had been captured by Fe_3O_4@Ag NPs-apt. So, the optimal dosage of Fe_3O_4@Ag NPs-apt in this experiment was 40 μL. In this experiment, 40 μL Fe_3O_4@Ag NPs-apt were used to enrich 1.0×10^7 CFU/mL *V. parahaemolyticus* solution, and the enrichment time ranging from 15 to 75 min were evaluated and compared as shown in Fig. 3b **and Fig S8**. The enrichment efficiency gradually increased with the increase of enrichment time. When the enrichment time was 60 min, the enrichment efficiency reached 95.41% and did not further improve significantly. So the best enrichment time was selected as 60 min for further analysis. The optimized Fe_3O_4@Ag NPs-apt dosage and enrichment time were used to determine the enrichment efficiency of certain concentrations of *V. parahaemolyticus*. Results are shown in Fig. 3c **and Fig S9**. Enrichment efficiency was only 32.11% for 1.0×10^8 CFU/mL *V. parahaemolyticus*. However, the enrichment efficiency of 1.0×10^7 CFU/mL, 1.0×10^6 CFU/mL, 1.0×10^5 CFU/mL and 1.0×10^4 CFU/mL *V. parahaemolyticus* were all more than 95%, which could meet the requirements of further experiment.

To improve the stability and IgY coupling efficiency of AuNPs, 0, 1, 3, 5, 7 and 9 μL of K_2CO_3 (0.1 mol/L) were added to evaluate and compare the pH of AuNPs solution. After modified with 30 μg IgY antibody, the color changes were observed, and the maximum absorption peak of the UV-Vis absorption spectrum was measured at wavelengths between 300 nm and 700 nm. The results are shown in **Fig S10**. When the volume of K_2CO_3 solution reached and exceeded 5 μL, the color of the solution remained red and didn't grow lighter due to aggregation. The peak value of the maximum absorption peak of the solution was highest when 7 μL K_2CO_3 was added, and the pH value of the solution at this time was 8.0 as determined by a pH meter, which was chosen as the optimal pH for AuNPs solution coupled with IgY. AuNPs-IgY with 5, 10, 15, 20 and 25 μg antibodies were evaluated and compared as shown in Fig. 3d. The difference between the experimental group and the sterile control group was the largest when the antibody coupling amount was 15 μg, which was selected as the optimal antibody coupling amount in this experiment. 10, 20, 30, 40 and 50 μL AuNPs-IgY were evaluated and compared as shown in Fig. 3e. The difference between the experimental group and the sterile control group was the largest when the usage of AuNPs-IgY was 40 μL, which was selected as the optimal usage of AuNPs-IgY in this experiment. Substrate color development time of 1, 3, 5, 7, 9, 11, 13 and 15 min were evaluated and compared as shown in Fig. 3f. The difference between the experimental group and the blank control group was the largest when the time was 7 min, which was selected as the optimal usage of substrate color development time for further analysis. Collectively, the optimal reaction conditions for the colorimetric sensing platform were determined as 40 μL Fe_3O_4@Ag NPs-apt, 60 min enrichment time, pH 8.0 for AuNPs-IgY conjugation with 15 μg IgY antibody, 40 μL AuNPs-IgY, and a 7 min substrate chromogenic

time, which collectively ensure the high efficiency, specificity and sensitivity of the platform for V. parahaemolyticus detection.

3.4. Sensitivity

Under the optimized experimental conditions, *V. parahemolyticus* concentrations from 10 to 10^7 CFU/mL were tested. As presented in Fig. 4a with the concentration of *V. parahemolyticus* increasing, the color of the solution changes from colorless to green, and the absorbance at 418 nm increases. There are two linear relationships between *V. parahemolyticus* concentration and the value of absorbance. One equation is A_{norm}=0.093lg*C*-0.053, with a correlation coefficient of R^2 = 0.990 (10 ~ 10^5 CFU/mL), another is A_{norm}=0.268lgC-0.927, with a correlation coefficient of R^2 = 0.992 (10^5~10^7 CFU/mL), which confirmed that the LOD was 3.02 CFU/mL.**Table S2** summarizes the performance comparison of the proposed method with previously reported assays for *V. parahaemolyticus* detection. Chen et al. (2021) developed a label-free colorimetric method with an LOD of 6.1×10² CFU/mL. Liu et al. (2018b) established a colorimetric immunoassay with a linear range of 20–10⁴ CFU/mL and an LOD of 15 CFU/mL. Qiao et al. (2024) reported a dual-substrate colorimetric system with an LOD of 1.12 CFU/mL and a range of 0–10⁴ CFU/mL. Wang et al. (2023) proposed a one-step label-free strategy with a quantitative LOD of 10³ CFU/mL. Zhang et al. (2024) designed a dual-mode immunosensor with a linear range of 1.0×10³–1.0×10⁸ CFU/mL and an LOD of 60 CFU/mL. Wu et al. (2015) developed an aptasensor with a range of 10–10⁶ CFU/mL and an LOD of 10 CFU/mL. Cheng et al. (2016) integrated PCR with colorimetry, achieving a range of 2.2×10⁵–3.4×10⁵ CFU/mL and an LOD of 2.9×10⁴ CFU/mL. Fu et al. (2018) presented a colorimetric immunoassay with a range of 10–10⁶ CFU/mL and an LOD of 10 CFU/mL. As indicated in **Table S2**, our method exhibits a lower LOD than most reported assays and a wider linear range than all comparative strategies. These results demonstrate the superior sensitivity and accuracy of the proposed detection system.

3.5. Specificity

The specificity of the proposed detection method was evaluated by comparing the responses toward *Staphylococcus aureus, Escherichia coli O157:H7, Listeria monocytogenes, Salmonella typhimurium*, with distilled water serving as the blank control instead of bacterial suspension. As illustrated in Fig. 5, the absorbance value of the *V. parahaemolyticus* - containing sample group at 418 nm was significantly higher than those of the blank control and other non-target bacterial groups. These results demonstrate that the developed detection system exhibits high specificity for *V. parahaemolyticus*, enabling effective discrimination from non-target microorganisms.

3.6. Analysis of Real Sample

To further explore and validate the practical applicability of the proposed method in complex food matrices, we applied it for the detection of *V. parahaemolyticus* at various concentrations in oyster samples, a typical seafood matrix frequently contaminated with this pathogen. As presented in Fig. 4b,

the absorbance intensity at 418 nm exhibits a concentration-dependent upward trend with the increase of *V. parahaemolyticus* levels. Notably, two distinct linear relationships were observed between the normalized absorbance (A) and the logarithm of V. parahaemolyticus concentration (lgC). The first linear regression equation is A = 0.086lgC − 0.029 (R^2 = 0.994) within the concentration range of 10 ~ 10^5 CFU/mL, while the second one is A = 0.236lgC − 0.735 (R^2 = 0.995) for the range of 10^5~10^7 CFU/mL. The excellent correlation coefficients (R^2 > 0.99) indicate the high reliability of the calibration curves. Based on these results, the limit of detection (LOD) of the method was calculated to be 54.95 CFU/mL, confirming its potential for sensitive quantification of *V. parahaemolyticus* in oyster samples. The results demonstrate that the detection limit for *V. parahaemolyticus* in simulated samples is higher than that in standard samples, with the slope of the standard curve in simulated samples being slightly lower. This may be attributed to the complex matrix interference in clams. However, the method's low detection limit and broad linear range indicate minimal interference from complex matrices in simulated samples, demonstrating strong anti-interference capability. These findings confirm the applicability of this analytical method for real sample testing.

4. Conclusion

In conclusion, we developed a pre-enrichment-free colorimetric sensing platform for rapid and quantitative detection of *V. parahaemolyticus* by integrating immunomagnetic specific capture, freeze-driven ssDNA modification and G-quadruplex DNAzyme-mediated signal amplification, where the Fe_3O_4@Ag NPs-apt/AuNPs-IgY sandwich system achieved efficient magnetic separation of target bacteria and the hairpin probe-triggered G-quadruplex DNAzyme formation realized sensitive signal conversion and amplification, effectively overcoming the drawbacks of complex pretreatment and low signal intensity in traditional detection methods; under optimized conditions, the platform exhibited two wide linear ranges (10 ~ 10^5 and 10^5~10^7 CFU/mL) with a low LOD of 3.02 CFU/mL in PBS and excellent specificity against common foodborne pathogens, and its successful application in oyster samples with a practical LOD of 54.95 CFU/mL verified good anti-interference ability and practical applicability in complex seafood matrices, demonstrating that this simple, sensitive and specific method is a promising on-site tool for *V. parahaemolyticus* detection in seafood, while the integration strategy also provides a novel design concept for constructing colorimetric sensors for other foodborne pathogens, and future work will focus on optimizing sample pretreatment to reduce matrix interference and improve real-sample detection sensitivity, as well as exploring system miniaturization to better meet on-site food safety monitoring demands.

Declarations

Acknowledgements

We would like to express our sincere gratitude to all the researchers who have provided invaluable support and assistance that facilitated the successful completion of this study. Special thanks are extended to the State Key Laboratory for Diagnosis and Treatment of Severe Zoonotic Infectious

Diseases, Key Laboratory for Zoonosis Research of the Ministry of Education, School of Public Health, Jilin University, China and the Department of Hygienic Inspection, School of Public Health, Jilin University for offering the essential experimental platforms, technical resources and favorable research environments for the conduct of this work. This work was financially supported by the National Natural Science Foundation of China and the Scientific and Technological Research Project of Jilin Province.

Funding This study was funded by the National Natural Science Foundation of China (Grant number 82103891,82373578) and the Scientific and Technological Research Project of Jilin Province (grant number:20250102253JC),Jilin University Undergraduate Training Program for Innovation and Entrepreneurship (202510183311)

Compliance with Ethical Standards

Ethical Approval This article does not contain any studies with human participants or animals performed by any of the authors.

Informed Consent Not applicable.

Conflict of Interest The authors declare no competing interests.

Data Availability declaration Not applicable**.**

References

1. Ma J Y, Zhu X K, Hu R G, Qi Z Z, Sun W C, Hao Z P, Cong W, Kang Y H (2023). A systematic review, meta-analysis and meta-regression of the global prevalence of foodborne Vibrio spp. infection in fishes: A persistent public health concern. Mar Pollut Bull [J], 187: 114521. https://doi.org/10.1016/j.marpolbul.2022.114521
2. Lovell C R (2017). Ecological fitness and virulence features of Vibrio parahaemolyticus in estuarine environments. Appl Microbiol Biotechnol [J], 101: 1781-1794.https://doi.org/10.1007/s00253-017-8096-9
3. Froelich B, Ayrapetyan M, Oliver J D (2013). Integration of Vibrio vulnificus into marine aggregates and its subsequent uptake by Crassostrea virginica oysters. Appl Environ Microbiol [J], 79: 1454-1458. https://doi.org/10.1128/aem.03095-12
4. Hash S, Martinez-Viedma M P, Fung F, Han J E, Yang P, Wong C, Doraisamy L, Menon S, Lightner D (2019). Nuclear magnetic resonance biosensor for rapid detection of Vibrio parahaemolyticus. Biomed J [J], 42: 187-192. https://doi.org/10.1016/j.bj.2019.01.009
5. Su Y C, Liu C C (2007). Vibrio parahaemolyticus: A concern of seafood safety. Food Microbiol [J], 24: 549-558.https://doi.org/10.1016/j.fm.2007.01.005
6. Velazquez-Roman J, León-Sicairos N, De Jesus Hernández-Díaz L, Canizalez-Roman A (2014). Pandemic Vibrio parahaemolyticus O3:K6 on the American continent. Front Cell Infect Microbiol [J],

3: 110. https://doi.org/10.3389/fcimb.2013.00110

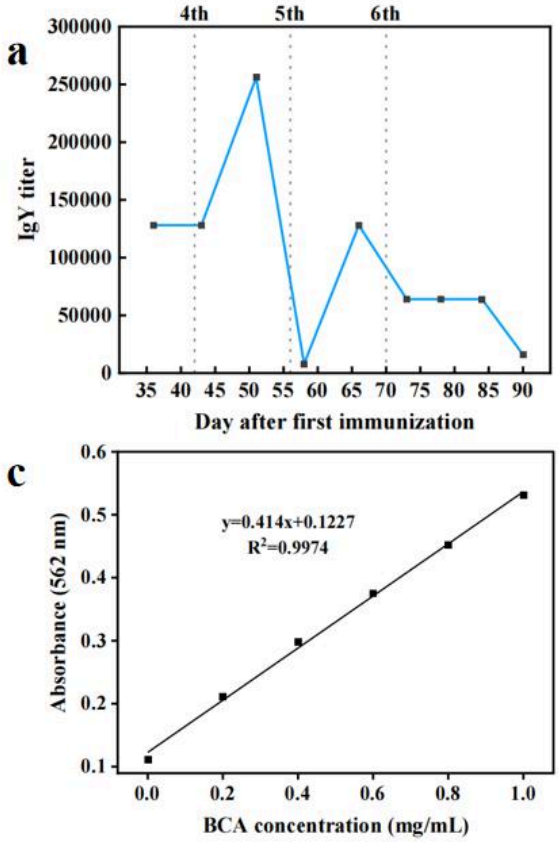
7. Zhao L, Chen H, Didelot X, Li Z, Li Y, Chen M, Du Y, Zhao H, Li J, Hu Q, Kan B, Chen M, Pang B (2020). Co-existence of multiple distinct lineages in Vibrio parahaemolyticus serotype O4:K12. Microb Genom [J], 6. https://doi.org/10.1099/mgen.0.000287
8. Anupama K P, Chakraborty A, Karunasagar I, Karunasagar I, Maiti B (2019). Loop-mediated isothermal amplification assay as a point-of-care diagnostic tool for Vibrio parahaemolyticus: recent developments and improvements. Expert Rev Mol Diagn [J], 19: 229-239. https://doi.org/10.1080/14737159.2019.1571913
9. Letchumanan V, Chan K G, Lee L H (2014). Vibrio parahaemolyticus: a review on the pathogenesis, prevalence, and advance molecular identification techniques. Front Microbiol [J], 5: 705.https://doi.org/10.3389/fmicb.2014.00705
10. Liu M, Chen S (2015). A novel adhesive factor contributing to the virulence of Vibrio parahaemolyticus. Sci Rep [J], 5: 14449.https://doi.org/10.1038/srep14449
11. Liu M, Yang S, Zheng C, Luo X, Bei W, Cai P (2018). Binding to type I collagen is essential for the infectivity of Vibrio parahaemolyticus to host cells. Cell Microbiol [J], 20: e12856.https://doi.org/10.1111/cmi.12856
12. Li M, Jiang Y, Shi X, Li Y, Jiang M, Lin Y, Qiu Y, Zuo L, Deng Y, Lin Z, Liao Y, Li Q, Hu Q (2019a). Simultaneous Identification of Clinically Common Vibrio parahaemolyticus Serotypes Using Probe Melting Curve Analysis. Front Cell Infect Microbiol [J], 9: 385.https://doi.org/10.3389/fcimb.2019.00385
13. Duan N, Wu S, Ma X, Xia Y, Wang Z (2014). A universal fluorescent aptasensor based on AccuBlue dye for the detection of pathogenic bacteria. Anal Biochem [J], 454: 1-6.https://doi.org/10.1016/j.ab.2014.03.005
14. Chen X, Wang L, He F, Chen G, Bai L, He K, Zhang F, Xu X (2021). Label-Free Colorimetric Method for Detection of Vibrio parahaemolyticus by Trimming the G-Quadruplex DNAzyme with CRISPR/Cas12a. Anal Chem [J], 93: 14300-14306.https://doi.org/10.1021/acs.analchem.1c03468
15. Wu S, Wang Y, Duan N, Ma H, Wang Z (2015). Colorimetric Aptasensor Based on Enzyme for the Detection of Vibrio parahemolyticus. J Agric Food Chem [J], 63: 7849-7854.https://doi.org/10.1021/acs.jafc.5b03224
16. Hu M, Yuan C, Tian T, Wang X, Sun J, Xiong E, Zhou X (2020). Single-Step, Salt-Aging-Free, and Thiol-Free Freezing Construction of AuNP-Based Bioprobes for Advancing CRISPR-Based Diagnostics. J Am Chem Soc [J], 142: 7506-7513.https://doi.org/10.1021/jacs.0c00217
17. Ye Y, Hou S, Wu X, Cheng X, He S (2022). Freeze-Driven Adsorption of Poly-A DNA on Gold Nanoparticles: From a Stable Biointerface to Plasmonic Dimers. Langmuir [J], 38: 4625-4632.https://doi.org/10.1021/acs.langmuir.2c00007
18. Zhu Y, Shen J, Zhou K, Chen C, Yang X, Li C (2011). Multifunctional Magnetic Composite Microspheres with in Situ Growth Au Nanoparticles: A Highly Efficient Catalyst System. Journal of Physical Chemistry C [J], 115: 1614-1619.https://doi.org/10.1021/jp109276q

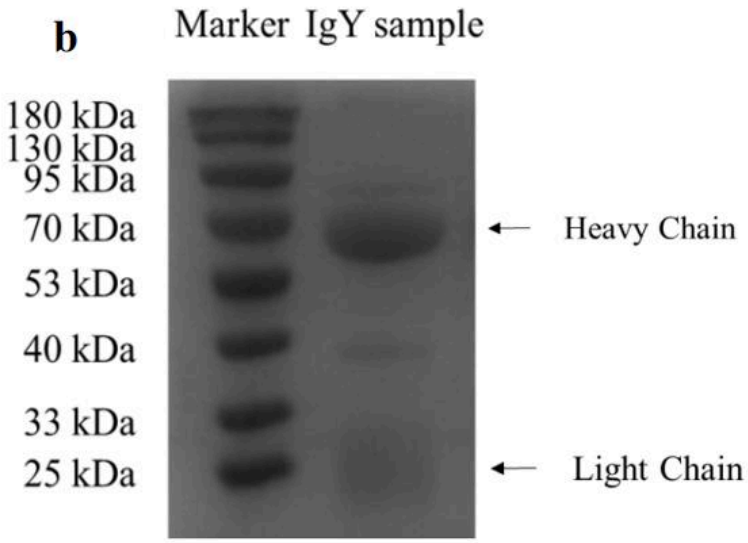
19. Su Z, Wei S, Shi X, Wang X, Zhang L, Bu X, Xu H, Liu Y, Jin M, Pang B, Zhao C (2023). Smartphone-assisted colorimetric detection of Salmonella typhimurium based on the catalytic reduction of 4-nitrophenol by β-cyclodextrin-capped gold nanoparticles. Anal Chim Acta [J], 1239: 340672. https://doi.org/10.1016/j.aca.2022.340672
20. Jun B H, Noh M S, Kim G, Kang H, Kim J H, Chung W J, Kim M S, Kim Y K, Cho M H, Jeong D H, Lee Y S (2009). Protein separation and identification using magnetic beads encoded with surface-enhanced Raman spectroscopy. Anal Biochem [J], 391: 24-30.https://doi.org/10.1016/j.ab.2009.05.005
21. Abbaspour A, Norouz-Sarvestani F, Noori A, Soltani N (2015). Aptamer-conjugated silver nanoparticles for electrochemical dual-aptamer-based sandwich detection of staphylococcus aureus. Biosens Bioelectron [J], 68: 149-155.https://doi.org/10.1016/j.bios.2014.12.040
22. Liu J, Lu Y (2006). Preparation of aptamer-linked gold nanoparticle purple aggregates for colorimetric sensing of analytes. Nat Protoc [J], 1: 246-252. https://doi.org/10.1038/nprot.2006.38
23. Li X, Zhao C, Liu Y, Li Y, Lian F, Wang D, Zhang Y, Wang J, Song X, Li J, Yang Y, Xu K (2019). Fluorescence signal amplification assay for the detection of B. melitensis 16M, based on peptide-mediated magnetic separation technology and a AuNP-mediated bio-barcode assembled by quantum dot technology. Analyst [J], 144: 2704-2715.https://doi.org/10.1039/c9an00028c
24. Zhou Y, Pan F G, Li Y S, Zhang Y Y, Zhang J H, Lu S Y, Ren H L, Liu Z S (2009). Colloidal gold probe-based immunochromatographic assay for the rapid detection of brevetoxins in fishery product samples. Biosens Bioelectron [J], 24: 2744-2747.https://doi.org/10.1016/j.bios.2009.01.034

Scheme 1

Scheme 1 is available in the Supplementary Files section.

Figures





d

Insert table. Results of IgY Concentration.

Antibody	Dilution	OD 562	SD	Concentration of IgY(mg/mL)
IgY sample	1:50	0.44	0.01	38.09

Figure 1

(a) Monitoring curve of IgY antibody titer; (b) SDS-PAGE for the IgY antibody; (c) Standard curve of BCA; (d) Results of IgY Concentration.

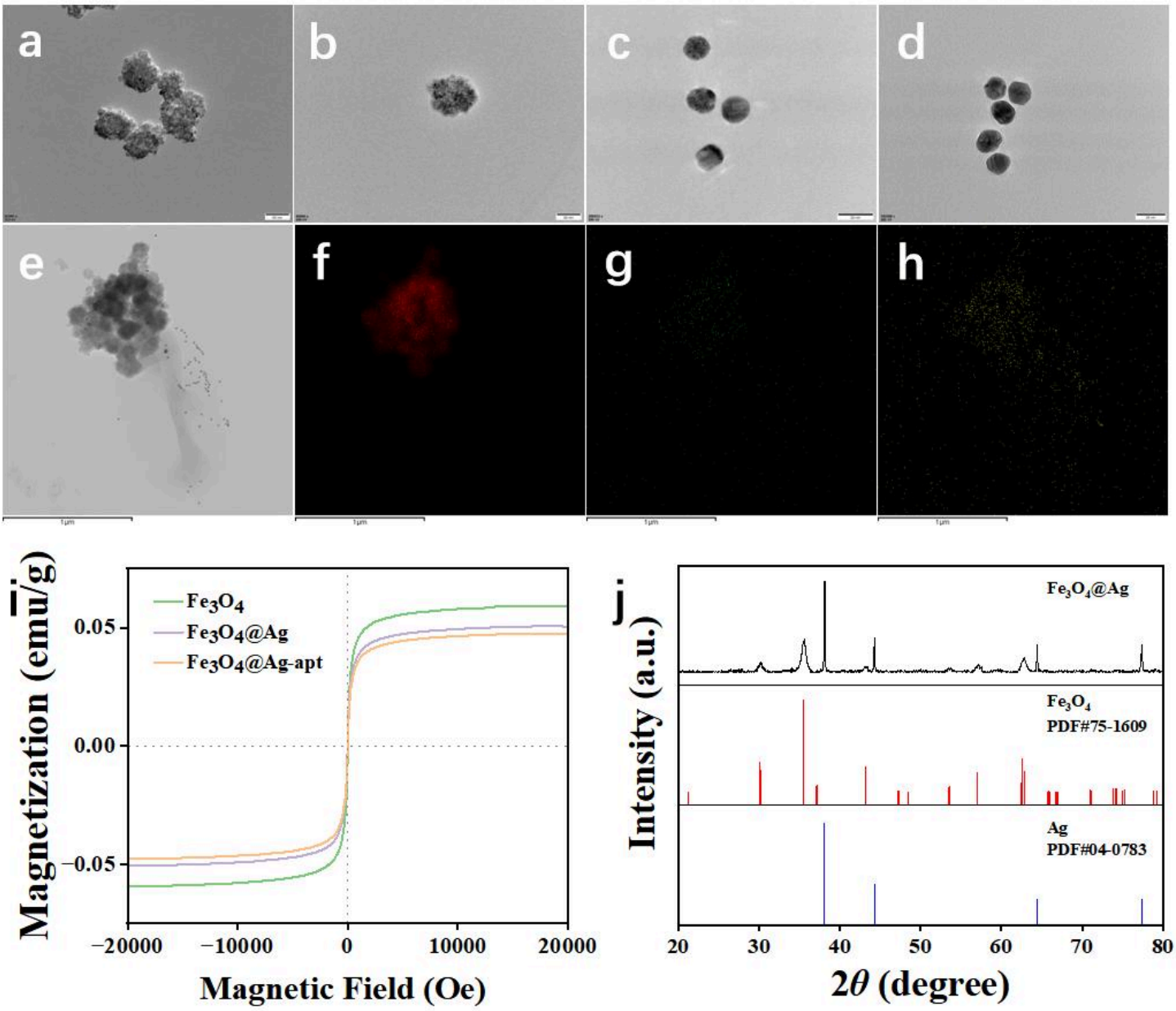


Figure 2

Characterization results.TEM: (a) Fe_3O_4@Ag NPs; (b) Fe_3O_4@Ag NPs - apt; (c) AuNPs; (d) AuNPs - IgY. (e - h) EDS map of element distribution of the three - sandwich structure. (i) VSM characterization of Fe_3O_4 NPs, Fe_3O_4@Ag NPs, and Fe_3O_4@Ag NPs - apt. (j) XRD characterization of Fe_3O_4@Ag NPs.

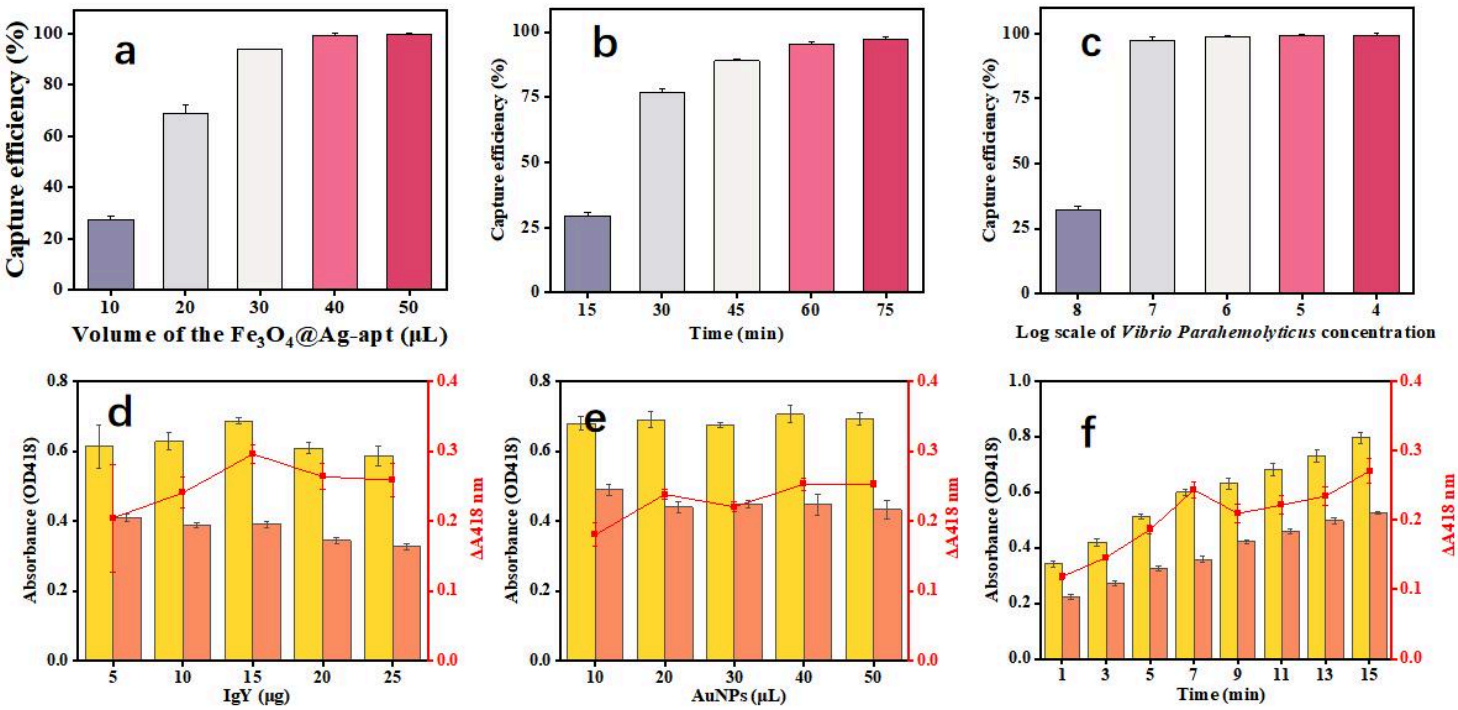


Figure 3

Optimization of (a) Fe_3O_4@Ag-apt dosage; (b) enrichment time; (c) bacterial concentration effects on enrichment efficiency. (d) antibody coupling amount;(e) dosages of AuNPs-IgY; (f) chromogenic time (The left is the experimental group, the right is the control group, and the red dot represents the difference between the two groups).Error bars represent the standard deviation of three replicates.

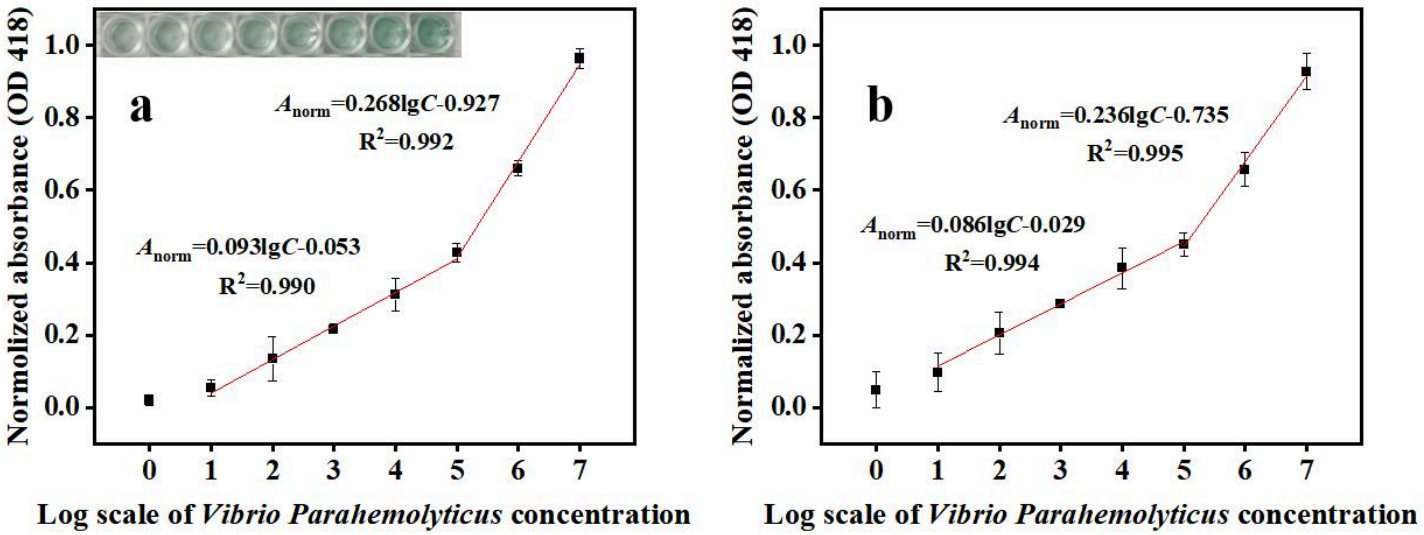


Figure 4

The normalized calibration curve for *V. parahaemolyticus***(a)**; **(b)**The normalized calibration curve for *V. parahemolyticus* in spiked oyster samples. (Anorm vs the logarithm of *V. parahaemolyticus* concentration) Error bars represent the standard deviation of three replicates.

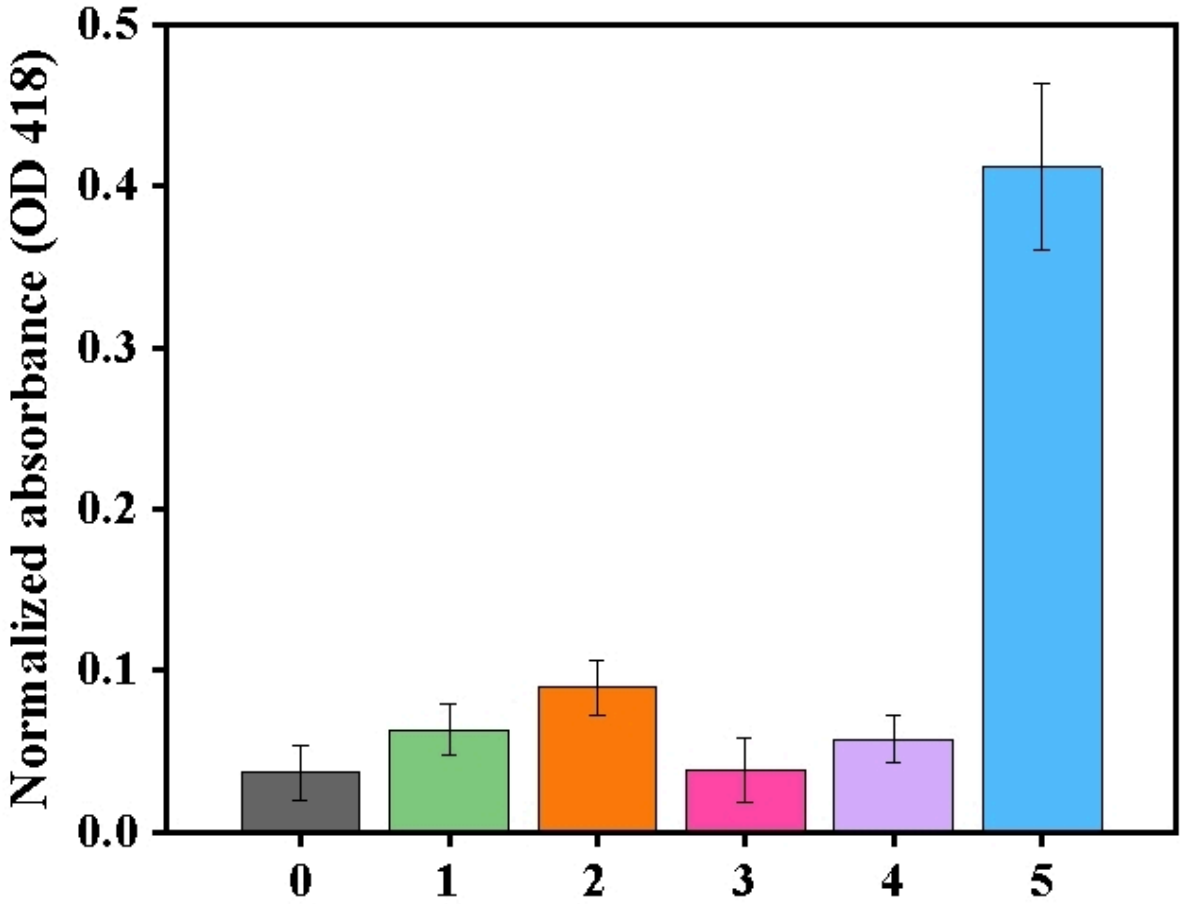


Figure 5

Results of specificity assessment. (0-5: Blank, *S.aureus, Ecoli.O157:H7, L.monocytogenes, S.typhimurium, V. parahemolyticus.*) The concentration of *V. parahemolyticus* was 1.0×10^4 CFU/mL. The concentration of non-target bacteria was 1.0×10^6 CFU/mL. Error bars represent the standard deviation of three replicates.

Supplementary Files

This is a list of supplementary files associated with this preprint. Click to download.

- Supportingmaterial.docx
- Graphicalabstract.jpg
- Scheme1.docx